



1 **Impacts of water partitioning and polarity of organic compounds on**
2 **secondary organic aerosol over Eastern China**

3 Jingyi Li^{1,2}, Haowen Zhang², Qi Ying^{3,*}, Zhijun Wu^{4,1}, Yanli Zhang^{5,6}, Xinming
4 Wang^{5,6,7}, Xinghua Li⁸, Yele Sun⁹, Min Hu^{4,1}, Yuanhang Zhang^{4,1}, Jianlin Hu^{1,2,*}

5 ¹ Collaborative Innovation Center of Atmospheric Environment and Equipment
6 Technology, Nanjing University of Information Science & Technology, Nanjing 210044,
7 China

8 ² Jiangsu Key Laboratory of Atmospheric Environment Monitoring and Pollution
9 Control, School of Environmental Science and Engineering, Nanjing University of
10 Information Science & Technology, Nanjing 210044, China

11 ³ Texas A&M University, College Station, Texas 77843, USA

12 ⁴ State Key Joint Laboratory of Environmental Simulation and Pollution Control, College
13 of Environmental Sciences and Engineering, Peking University, Beijing 100871, China

14 ⁵ State Key Laboratory of Organic Geochemistry and Guangdong Key Laboratory of
15 Environmental Protection and Resources Utilization, Guangzhou Institute of
16 Geochemistry, Chinese Academy of Sciences, Guangzhou 510640, China

17 ⁶ Center for Excellence in Regional Atmospheric Environment, Institute of Urban
18 Environment, Chinese Academy of Sciences, Xiamen 361021, China

19 ⁷ University of Chinese Academy of Sciences, Beijing 100049, China

20 ⁸ School of Space & Environment, Beihang University, Beijing 100191, China

21 ⁹ State Key Laboratory of Atmospheric Boundary Layer Physics and Atmospheric
22 Chemistry, Institute of Atmospheric Physics, Chinese Academy of Sciences, Beijing
23 100029, China

24

25 Corresponding authors:

26 Qi Ying, Email: qying@civil.tamu.edu

27 Jianlin Hu, Email: jianlinhu@nuist.edu.cn

28



29 **Abstract**

30 Secondary organic aerosol (SOA) is an important component of fine particular matter
31 (PM_{2.5}) in China. Most air quality models use an equilibrium partitioning method along
32 with estimated saturation vapor pressure of semi-volatile organic compounds (SVOCs) to
33 predict SOA formation. However, this method ignores partitioning of water vapor to the
34 organic aerosols and the organic phase non-ideality, both of which affect the partitioning
35 of SVOCs. In this study, the Community Multi-scale Air Quality model (CMAQv5.0.1)
36 was used to investigate the above impacts on SOA formation during winter (January) and
37 summer (July) of 2013 over eastern China. The organic aerosol module was updated by
38 incorporating water partitioning into the organic particulate matter (OPM) and considering
39 non-ideality of organic-water mixture. The modified model can generally capture the
40 observed organic carbon (OC), the total organic aerosol (OA) and diurnal variation of PM_{2.5}
41 at ground sites. SOA concentration shows significant seasonal and spatial variations, with
42 high concentration levels in North China Plain (NCP), Central China and Sichuan basin
43 (SCB) areas during winter (up to 25 μg m⁻³) and in Yangtze River Delta (YRD) during
44 summer (up to 12 μg m⁻³). When water partitioning is included in winter, SOA
45 concentrations increase slightly, with the monthly-averaged daily maximum relative
46 difference of 10-20% at the surface and 10-30% for the whole column, mostly due to the
47 increase in anthropogenic SOA. The increase in SOA is more significant in summer, by
48 20-90% at the surface and 30-70% for the whole column. The increase of SOA over the
49 land is mostly due to biogenic SOA while the increase of SOA over the coastal regions is
50 related with that of anthropogenic origin. Further analysis of two representative cities, Jinan
51 and Nanjing, shows that changes of SOA are favored under hot and humid conditions. The
52 increases in SOA cause a 12% elevation in the aerosol optical depth (AOD) and 15%
53 enhancement in the cooling effects of aerosol radiative forcing (ARF) over YRD in summer.
54 The aerosol liquid water content associated with OPM (ALW_{org}) at the surface is relatively
55 high over the land in winter and over the ocean in summer, with the monthly-averaged



56 daily maximum of 2-9 and 5-12 $\mu\text{g m}^{-3}$, respectively. By using the κ -Köhler theory, we
57 calculated the hygroscopicity of OA with modeled ALW_{org} , finding that the correlation
58 with O:C ratio varies significantly across different cities and seasons. Water partitioning
59 into OPM only promotes SOA formation, while non-ideality of organic-water mixture only
60 leads to decreases in SOA in most regions of eastern China. Water partitioning into OPM
61 should be considered in air quality models in simulating SOA, especially in hot and humid
62 environments.

63

64 **Keywords:** SOA, non-ideality, water partitioning, hygroscopicity

65

66 **1 Introduction**

67 Secondary organic aerosol (SOA) is formed via a complex interaction of volatile organic
68 compounds (VOCs) with oxidants and primary particles emitted from anthropogenic and
69 biogenic sources in the atmosphere. As an important component of fine particulate matter
70 ($\text{PM}_{2.5}$), SOA can cause severe air pollution in urban and suburban areas (Huang et al.,
71 2014) and exhibit adverse health effects (Polichetti et al., 2009;Feng et al., 2016;Xing et
72 al., 2016;Atkinson et al., 2014). SOA also plays an important role in new particle formation
73 and particle growth (Man et al., 2015;Zhang et al., 2011;Wiedensohler et al., 2009;Yue et
74 al., 2011;Liu et al., 2014;Ehn et al., 2014;Huang et al., 2019;Jokinen et al., 2015) and
75 further contributes to the enhancement of cloud condensation nuclei (CCN) (Yue et al.,
76 2011;Wiedensohler et al., 2009;Liu et al., 2014;Jokinen et al., 2015). This will, in turn,
77 impact the atmospheric aerosol burden, precipitation and water circulation, solar radiation
78 budget, and climate (Rosenfeld et al., 2008;Spracklen et al., 2011;Quaas et al.,
79 2008;Ramanathan et al., 2001;Hatzianastassiou et al., 2007;Hegerl et al., 2015). However,
80 the mechanisms of these influences are not well understood so far, due to the high
81 uncertainties associated with the formation and physical and chemical properties of SOA
82 (Shrivastava et al., 2017). Large gaps still exist in SOA mass loadings and properties



83 between model estimates and laboratory and field measurements (Gentner et al.,
84 2017;Ervens et al., 2011;Hayes et al., 2015). Therefore, it is crucial to explore and resolve
85 this issue to improve our knowledge of the roles of SOA in the environment, health, and
86 climate.

87 Gas-particle partitioning of semi-volatile and low-volatile organic compounds
88 generated from VOC oxidation is an important pathway of SOA formation. In most current
89 chemical transport models (CTMs), this process is treated as an equilibrium partitioning
90 that depends on the mass concentration of organic particulate matter (OPM), ambient
91 temperature, the mean molecular weight of OPM, and the volatility of purer condensed
92 organics (Pankow, 1994). The volatilities of condensed organic products from a certain
93 precursor VOC are either represented by that of several lumped surrogates based on
94 chamber experiments (2-product model) (Odum et al., 1996) or fitted into different bins of
95 a fixed volatility range (usually $0.01\text{-}10^5 \mu\text{g m}^{-3}$) (volatility basis set model, VBS model)
96 (Donahue et al., 2006). Although the above models can capture the general trend of SOA
97 evolution and mass concentration to some extent (Slowik et al., 2010;Li et al., 2017a;Baek
98 et al., 2011;Bergström et al., 2012;Woody et al., 2016;Heald et al., 2006), both of them
99 neglected two key factors that may lead to biases: 1) the structures and interactions of
100 condensed organics (non-ideality); 2) partitioning of water vapor, an abundant atmospheric
101 constituent to OPM. The non-ideality alters the volatility of condensed organics, and thus
102 their contributions to the total SOA mass loading (Cappa et al., 2008). Water partitioning
103 into OPM can reduce the partial pressure of organics and lead to increase in SOA mass,
104 which is called the Raoult's Law effect (Prisle et al., 2010). This impact may vary for
105 different SOA precursors (Healy et al., 2009;Prisle et al., 2010). The above two aspects
106 will not only affect the chemical composition of SOA but also the inorganic portion (Ansari
107 and Pandis, 2000;Meyer et al., 2009) and optical properties (Liu and Wang, 2010;Denjean
108 et al., 2015) of aerosols.



109 Laboratory and field studies have confirmed the fact that water absorbed by SOA
110 (quantified as hygroscopicity, κ) from a variety of VOCs (Lambe et al., 2011;Zhao et al.,
111 2016b;Asa-Awuku et al., 2010;Varutbangkul et al., 2006). The hygroscopicity of SOA is
112 highly correlated with the oxygen-to-carbon ratio (O:C) and increases with more oxidized
113 SOA during photochemical aging (Poulain et al., 2010;Wang et al., 2014;Lambe et al.,
114 2011;Tritscher et al., 2011a;Zhao et al., 2016b;Massoli et al., 2010;Tritscher et al.,
115 2011b;Duplissy et al., 2011). The OPM-associated water partitioning can be estimated
116 using the κ -Köhler theory under the Zdanovskii-Stokes-Robinson (ZSR) assumption of no
117 interactions between any constituents in aerosols (Petters and Kreidenweis, 2007). The total
118 water content is the summarization of each constitute at the same RH. Guo et al. (2015)
119 found that this simplified method, along with the ISORROPIA model which is used to
120 predict aerosol liquid water (ALW) associated with the inorganic portion of aerosols,
121 reproduced the observed total ALW in the ambient environment. Pye et al. (2017) applied
122 this approach along with a parameterization of overall κ based on O:C ratio and a
123 simplified method to estimate activity coefficients of organics and found that modeled OA
124 and ALW are improved during daytime but still biased low at nighttime. Shortcomings still
125 exist in the above method for water associated organics (ALW_{org}) as interactions between
126 organic species in the organic-water mixture are not considered, which has been shown to
127 play an important role in SOA formation and water partitioning to OPM (Kim et al., 2019).
128 A representation of water partitioning along with SVOCs with consideration of water-
129 organic and organic-organic interactions in CTMs showed significant influences in SOA
130 and ALW in the eastern U.S. where biogenic SOA dominated in OA and the internal mixing
131 assumed for the aerosol (Pankow et al., 2015;Jathar et al., 2016).

132 China has been suffering from severe $PM_{2.5}$ pollution especially in the eastern region
133 with fast urbanization and economic development (Guo et al., 2014;Fu and Chen,
134 2017;Yang et al., 2016). The secondary portion has been proved to be dominated in $PM_{2.5}$
135 and organic aerosol increases during haze events (Huang et al., 2014;Sun et al., 2019). In



136 addition, SOA is a very important component of PM_{2.5} in China that contributes about 20-
137 50% (Li et al., 2017b). Previous modeling studies indicated that SOA was underpredicted
138 in this region (Wang et al., 2011; Lin et al., 2016; Jiang et al., 2012) and the impacts of non-
139 ideality and water-OPM partitioning have not been evaluated.

140 In this study, regional simulations of SOA during January and July of 2013 over
141 eastern China under several scenarios were conducted to investigate the seasonal variation
142 of SOA due to water partitioning into OPM. Model performances were firstly evaluated
143 against observed meteorological parameters (temperature and relative humidity) as well as
144 PM_{2.5}, OC, and OA at ground monitoring sites. Then, the regional and seasonal impacts on
145 SOA and water content were quantified. Factors related to the impacts on SOA, including
146 sources of precursors, chemical compositions and meteorological conditions were further
147 analyzed. Lastly, the impacts on aerosol optical properties and hygroscopicity were
148 investigated.

149 **2 Methodology**

150 The Community Multi-scale Air Quality model (CMAQ v5.0.1) coupled with a modified
151 SAPRC-11 was used in this study. Model configurations were largely based on that used
152 by Hu et al. (2016) as summarized below. Firstly, SAPRC-11 was expanded for more
153 detailed treatment of isoprene oxidation and tracking dicarbonyl (glyoxal and
154 methylglyoxal) products from different groups of major precursors (Ying et al., 2015);
155 Secondly, heterogeneous formation of secondary nitrate and sulfate from NO₂ and SO₂
156 reaction on particle surface (Ying et al., 2014), and SOA from isoprene epoxydiols
157 (IEPOX), methacrylic acid epoxide (MAE) and dicarbonyls through surface-controlled
158 reactive uptake (Li et al., 2015; Pankow et al., 2015) were added; Thirdly, SOA yields were
159 corrected for vapor wall loss (Zhang et al., 2014).

160 Two types of SOA were considered in the current model, “semi-volatile” (SV) portion
161 that formed via equilibrium absorption-partitioning of SVOCs, and “non-volatile” (NV)
162 portion that formed via direct oxidation of aromatics at low-NO_x, isoprene oxidation
under



163 acidic conditions, reactive uptake of dicarbonyls, IEPOX and MAE, and oligomers. The
164 SV-SOA module mostly based on that of Pankow et al. (2015) with several updates in the
165 treatment of primary organic aerosol (POA) by including it in the non-ideality calculation
166 of the organic-water mixture. The mass distribution of SVOCs between the gas-phase and
167 particle-phase follows the equation:

$$K_{p,i} = \frac{F_i}{M \cdot A_i} \quad (\text{Eq 1})$$

168 where $K_{p,i}(\text{m}^3 \mu\text{g}^{-1})$ is the gas/particle partitioning constant for compound i , $F_i(\mu\text{g m}^{-3})$
169 is the concentration of species i in the particle phase, $A_i(\mu\text{g m}^{-3})$ is the concentration of
170 species i in the gas phase, and $M(\mu\text{g m}^{-3})$ is the total mass concentration of the absorbing
171 phase. The gas/particle partitioning constant $K_{p,i}$ is dependent on the composition of the
172 absorbing organic phase. Pankow et al. (1994) derived $K_{p,i}$ for SVOCs partitioning into
173 an absorbing organic phase as:

$$K_{p,i} = \frac{RT}{10^6 \overline{MW} \xi_i p_{L,i}^o} \quad (\text{Eq 2})$$

174 where $p_{L,i}^o(\text{atm})$ is the saturation vapor pressure of the pure compound i at temperature
175 $T(\text{K})$, ξ_i is the activity coefficient of species i in the absorbing organic phase, \overline{MW} (g mol^{-1})
176 is the average molecular weight of the absorbing organic phase, R ($8.314 \text{ J mol}^{-1} \text{ K}^{-1}$) is
177 the gas constant, and 10^6 is used to convert the unit to $\text{m}^3 \mu\text{g}^{-1}$.

178 There are 12 lumped SVOCs generated by oxidation of alkanes, alkenes, and
179 aromatics oxidized under different NO_x conditions (Table S1). Activity coefficients of
180 SVOCs were calculated based on the composition of absorbing organic phase using the
181 UNiversal Functional Activity Coefficient (UNIFAC) method (Fredenslund et al., 1975),
182 with assigned carbon number (n_c), functional groups and energy interaction parameters to
183 both SV and NV compounds (Pankow et al., 2015). The UNIFAC model is one of the
184 commonly used models that activity coefficients of condensed organics and their
185 interactions with water can be estimated. This method has been adopted to investigate the
186 impacts of non-ideality and water-OPM partitioning on SOA for different precursors in



187 box models (Seinfeld et al., 2001; Bowman and Melton, 2004) and CTMs (Jathar et al.,
188 2016; Pankow et al., 2015; Kim et al., 2019). The primary organic aerosols (POA) was
189 assumed to have a bulk composition of ten categories of surrogate species (Table S3), as
190 used by Li et al. (2015). POA is also involved in the calculation of activity coefficients for
191 the organics in the condensed phase. Detailed information about the surrogate species
192 including the structures and properties can be found in Li et al. (2015) and references
193 therein.

194 In addition to organic compounds, water partitioning into OPM is enabled according
195 to Eq 1 and Eq 2. In such a case, the absorbing phase in Eq 1 includes both organic aerosols
196 and water partitioning into OPM. As water considered in the absorbing phase, it will further
197 alter the molar fraction of each composition, the activity coefficient of SVOCs and the SV-
198 SOA mass concentrations as a result.

199 As the water partitioning into OPM is highly correlated with the hygroscopicity of
200 aerosols (κ), their correlation can be expressed by the κ -Köhler theory with Kelvin effect
201 neglected (Peter et al., 2006):

$$ALW_{org} = V_{org} \kappa_{org} \frac{a_w}{1 - a_w} \quad (\text{Eq3})$$

202 where V_{org} is the volume concentration of organic, and a_w is the water activity (assumed to
203 be the same as RH). Taken the density of organic aerosol to be 1.2 g cm^{-3} (Li et al., 2019),
204 the hygroscopicity of the total OA can be estimated. This simplified method can be used to
205 estimate OPM associated water (Guo et al., 2015; Li et al., 2019). In addition, the
206 hygroscopicity of organic aerosol is dependent on the degree of oxygenation, showing a
207 positive linear relationship with the O:C ratio (Massoli et al., 2010; Duplissy et al.,
208 2011; Lambe et al., 2011; Hong et al., 2018; Li et al., 2019). We therefore estimated the
209 correlation of κ and O:C ratio at 9 representative cities during January and July with the
210 reduced major axis regression method (Ayers, 2001). O:C ratio of the total OA was
211 calculated as following:



$$O:C = \sum_{i=1}^n f_i (O:C)_i \quad (\text{Eq4})$$

212 where f_i and $(O:C)_i$ are the molar fraction and O:C ratio of organic aerosol component
213 i . For POA, a fixed molar fraction and composition has been assumed following Li et al.
214 (2015). For SOA, the O:C ratio was estimated by their OM:OC ratio (Simon and Bhawe,
215 2012):

$$O:C = \frac{12}{15} (\text{OM:OC}) - \frac{14}{15} \quad (\text{Eq5})$$

216 OM:OC ratio of each SOA component follows Pye et al. (2017).

217 The simulation domain has a horizontal resolution $36 \text{ km} \times 36 \text{ km}$ and a vertical
218 structure of 18 layers up to 21 km, which covers eastern China as shown in Figure S1.
219 Anthropogenic emissions were generated from the Multi-resolution Emission Inventory for
220 China (MEIC) (Zhang et al., 2009; Li et al., 2014; Zheng et al., 2014; Liu et al., 2015) v1.0
221 with a $0.25^\circ \times 0.25^\circ$ resolution (<http://www.meicmodel.org>) for China, and the Regional
222 Emission inventory in Asia version 2 (REAS2) (Kurokawa et al., 2013) with a $0.25^\circ \times 0.25^\circ$
223 resolution (<http://www.nies.go.jp/REAS/>) for the rest of the domain. Biogenic emissions
224 were generated by the Model for Emissions of Gases and Aerosols from Nature (MEGAN)
225 v2.1, with the leaf area index (LAI) from the 8- day Moderate Resolution Imaging
226 Spectroradiometer (MODIS) LAI product (MOD15A2) and the plant function types (PFTs)
227 from the Global Community Land Model (CLM 3.0). Open biomass burning emissions
228 were generated from the Fire Inventory from NCAR (FINN) (Wiedinmyer et al., 2011).
229 Dust and sea salt emissions were generated in line during CMAQ simulations.
230 Meteorological fields were generated using the Weather Research and Forecasting (WRF)
231 model v3.6.1 with initial and boundary conditions from the NCEP FNL Operational Model
232 Global Tropospheric Analyses dataset. More details about the model application can be
233 found in Hu et al. (2016)

234 Four scenarios are investigated in this study. The base case (BS) that applied the
235 default secondary organic aerosol module of CMAQ; the water case (S1) that only water



236 partitioning into OPM was considered; the UNIFAC case (S2) that effects of molecular
237 structure of the primary and secondary organic species were included; and the combined
238 case (S3) that S1 and S2 were combined together.

239 **3 Results**

240 **3.1 Model evaluation**

241 Temperature and relative humidity (RH) are the two meteorological factors that affect SOA
242 formation. Table 1 shows the comparison of WRF predictions and observations in 8 sub-
243 regions of the domain (Figure S1). Observed data are accessible from the National Climatic
244 Data Center at <ftp://ftp.ncdc.noaa.gov/pub/data/noaa>. Temperature and RH are well
245 captured by WRF in YRD, the Pearl River Delta (PRD), and central regions of China (the
246 major regions of eastern China). Model estimates of daily organic carbon (OC) from the
247 BS case were compared with measurements at monitoring sites in Beijing and Guangzhou
248 during the winter of 2013 (Figure 1(a)). Overall, the ratio between modeled and observed
249 OC concentration falls in the range of 1:2 to 2:1, with a correlation coefficient R of 0.70.
250 The model tends to underestimate OC, especially in Beijing on highly polluted days (by -
251 37~48%). No significant improvements to modeled OC were observed in S3. The impacts
252 of water co-condensation and polarity of organic condensed species on SOA exhibit strong
253 seasonal and spatial features, which are further discussed in Section 4. The impacts in
254 Beijing and Guangzhou are not significant during winter. The bias in OC might be due to
255 under-estimated POA emissions and under-predicted SOA in CMAQ from missing
256 precursors (Hu et al., 2017; Zhao et al., 2016a).

257 The model estimate of OA was further investigated. As shown in Figure 1(b), CMAQ
258 can well capture the observed diurnal variation of OA at Beijing during wintertime, except
259 for the underestimates of peak values. A better agreement between the model and the
260 observations is observed on non-polluted days (daily-averaged concentration less than 75
261 $\mu\text{g m}^{-3}$). The monthly-averaged mean fractional bias (MFB) and mean fractional error
262 (MFE) are -0.13 and 0.27, respectively. POA is the primary contributor to OA at Beijing



263 in winter, accounting for 88% due to aging of POA not treated in the current model. The
264 fraction of SOA is small, resulting in little impacts on SOA by water partitioning into OPM
265 and insignificant improvements of the modeled OA in S3.

266 Figure S2 shows the comparison of modeled and observed $PM_{2.5}$ at monitoring sites
267 as shown in Figure S1 (a) during July of 2013. Generally, our model can well reproduce
268 the diurnal variation of $PM_{2.5}$ in most regions. Predicted $PM_{2.5}$ on high concentration days
269 are biased low compared to observations, especially in the North Central Plain (NCP). The
270 NCP region has the highest $PM_{2.5}$ from $60 \mu\text{g m}^{-3}$ to $300 \mu\text{g m}^{-3}$ compared to other regions.
271 The bias in modeled $PM_{2.5}$ is significant in cities in the Northwest. This might be due to
272 missing dust emissions in the current inventory (Hu et al., 2016). To further evaluate the
273 model performance, statistics of MFB and MFE were plotted against observed $PM_{2.5}$
274 concentration at all monitoring sites (Figure S3). The criteria and goal followed
275 recommendations of Boylan and Russell (2006). Our model performed well as most of the
276 predictions meet the criteria and a large fraction (>58%) meet the goal. The averaged MFB
277 and MFE are -0.28 and 0.39 respectively, indicating slightly underestimate of $PM_{2.5}$ by the
278 model.

279 **3.2 Impacts of water partitioning on SOA**

280 Distribution of SOA varied greatly in the two seasons. In winter, SOA is relatively high in
281 eastern SCB and in the contiguous areas of Shandong, Henan, Anhui, and Hubei provinces
282 (Figure 2 and Figure S4). Monthly-averaged SOA concentrations in the above two areas
283 are up to 25 and 15-20 $\mu\text{g m}^{-3}$, respectively. The major precursors of SOA are originated
284 from anthropogenic sources such as dicarbonyl products of aromatics oxidation, xylenes
285 and toluene (Figure S5). In summer, surface SOA is high in NE, NCP and YRD regions.
286 Shanghai, Jiangsu province and coastal areas of Yellow Sea show the highest SOA of ~9-
287 12 $\mu\text{g m}^{-3}$ at the surface and ~20 mg m^{-2} as the column total (col-SOA) in the atmosphere
288 below 21 km (Figure S4). Different from winter SOA, a significant fraction of summer



289 SOA is originated from biogenic emissions in Shanghai and Jiangsu province (Figure S5).
290 Anthropogenic SOA is high in July in coastal areas of Yellow Sea and Bohai Bay.

291 Combined effects of water partitioning into OPM and non-ideality on SOA formation
292 (S3) also exhibit strong seasonal variation. In winter, the increase of SOA is relatively
293 small, by $\sim 1\text{--}4\ \mu\text{g m}^{-3}$ (10-20%) at the surface (Figure 2) and less than $\sim 5\ \text{mg m}^{-2}$ (10-30%)
294 as for the column concentration (Figure S4). The influences on SOA also differ in different
295 altitudes. For example, the maximum increment at the surface is observed in Shandong
296 province in NCP (Figure 2), while SOA at higher levels of the atmosphere is more
297 significant in South China (Figure S4). The increase in SOA is mostly attributed to
298 anthropogenic sources in winter (Figure S5 and S7). In summer, higher temperature and
299 relative humidity (RH) promote SOA formation as well as water partitioning into OPM. At
300 the surface, SOA increases by $3\text{--}9\ \mu\text{g m}^{-3}$ (40-50%) in coastal areas and $2\text{--}9\ \mu\text{g m}^{-3}$ (20-
301 90%) over the land, which are dominated by anthropogenic and biogenic origin,
302 respectively (Figure S6). For col-SOA, in addition to coastal areas, more significant
303 increase is observed in YRD, most of Henan province, and the contiguous areas of Hubei,
304 Hunan, and Jiangxi province (Figure S4) by about 30-70%.

305 Regional distribution of water partitioning into OPM is similar to the changes of SOA.
306 Figure 3 shows the regional distribution of monthly-averaged daily maximum ALW_{org} . We
307 see up to $9\ \mu\text{g m}^{-3}$ ALW_{org} at surface occurs in Shandong in winter where great increment
308 in SOA appears as well. In other areas, ALW_{org} is about $2\text{--}6\ \mu\text{g m}^{-3}$. The ratio of ALW_{org}
309 to SOA is about 0.1-0.5 in winter. In summer, water partitioning mostly involves in east
310 coastal areas at the surface where significant increase of anthropogenic SOA (such as
311 toluene and xylenes) is observed. This might be due to the high polarity of anthropogenic
312 SVOCs (having more -COOH groups) that absorb more water. In the coastal areas, ALW_{org}
313 is about $5\text{--}12\ \mu\text{g m}^{-3}$, with a ratio to SOA of 0.3-0.6. ALW_{org} over the land is about $2\text{--}7\ \mu\text{g}$
314 m^{-3} ($\text{ALW}_{\text{org}}/\text{SOA}$ ratio of 0.1-0.4) in most areas, which is mostly associated with the
315 increase of BSOA such as isoprene and monoterpenes with abundant OH group in SVOCs.



316 The highest ALW_{org} is $16 \mu\text{g m}^{-3}$ near Shanghai (ALW_{org}/SOA ratio of 0.57). Water
317 partitioning also varies at different altitudes (Figure S9). In winter, more column water
318 partitions into OPM ($col-ALW_{org}$) in Chongqing, Hunan, Guanxi, Guangdong and Guizhou
319 province, with the $col-ALW_{org}/col-SOA$ ratio of 0.2-0.3. In summer, higher $col-ALW_{org}$
320 is predicted over the land, especially in YRD, with the $col-ALW_{org}/col-SOA$ ratio of 0.1-
321 0.3 over eastern China.

322 Figure 4 shows the correlation of κ_{org} with O:C ratio. The estimated O:C ratio is
323 within the range of 0.2-0.6. In summer, the oxidation state of OA shows different degrees
324 of enhancement compared to winter at most of the cities except Guangzhou, due to
325 increased contribution of SOA to total OA. The averaged κ_{org} of OA in each O:C bin
326 falls in the range of 0.001-0.1, with the highest κ_{org} (~ 0.3) at Beijing in summer. The
327 linear correlation between κ_{org} and O:C shows significant spatial and seasonal variations.
328 For example, the slope of κ_{org} -O:C is much smaller in winter (45-74% less) than in
329 summer in the Northern cities such as Shenyang, Beijing, Zhengzhou, and Xi'an, while the
330 slope of κ_{org} -O:C in winter is much higher (47-104% more) than in summer in the
331 Southern cities, such as Nanjing, Chengdu and Guangzhou. In Jinan and Shanghai, the
332 slope is quite similar in both seasons. The fitted correlations are very different from
333 previous studies with a relatively higher slope of κ_{org} -O:C from 0.18 to 0.37 (Duplissy et
334 al., 2011; Lambe et al., 2011; Massoli et al., 2010; Chang et al., 2010), indicating the
335 hygroscopicity of aerosols with chemical complexity cannot be simply represented by a
336 single parameter such as O:C (Rickards et al., 2013).

337 **3.3 Impacts on solar radiation**

338 The impacts on aerosol optical depth (AOD) and aerosol radiative forcing (ARF) were
339 further investigated. Figure 5 shows the monthly-averaged AOD at 550 nm in January and
340 July of 2013. It was calculated as the accumulation of model estimated extinction
341 coefficient of fine particles (EXT_i) multiplied by the thickness (HL_i) of each layer:



$$\text{AOD} = \sum_{i=1}^N \text{EXT}_i \times \text{HL}_i \quad (\text{Eq6})$$

342 Where N is the number of layers. There are two methods to estimate the aerosol extinction
343 coefficient in CMAQ. One is using the Mie theory (EXT_m), and the other is based on
344 extinction values from the IMPROVE monitoring network that considers the impacts of
345 hygroscopicity of different aerosol components (EXT_r) (Malm et al., 1994). AOD calculated
346 with the two types of extinction coefficient are denoted as AOD_m and AOD_r , respectively.

347 In Figure 5, a clear pattern of high AOD_r in SCB and NCP and low AOD_r in west
348 China in both winter and summer is observed, consistent with previous studies (He et al.,
349 2019; He et al., 2016; Luo et al., 2014). An identified trend in AOD_m is observed as shown
350 in Figure S10. The monthly-averaged AOD_r ranges from 1.1 to 3.5 in January and from 0.4
351 to 0.8 in July. AOD_m is lower than AOD_r , falling in 0.7-2.2 in January and 0.3-0.6 in July.
352 The model significantly overestimates AOD in January but agrees better with observations
353 from MODIS in the high regions in July (Figure S11). Biases in the predicted AOD might
354 be partially due to the empirical equation applied in the calculation of AOD in CMAQ
355 (Wang et al., 2009; Liu et al., 2010), and partially due to the uncertainties of fine AOD
356 overland from MODIS data (Wang et al., 2009; Levy et al., 2010). With water partitioning
357 into OPM, changes in SOA mass concentration and chemical composition lead to increase
358 of AOD, which shows a strong spatial and seasonal pattern. In winter, there is no significant
359 increase in AOD_r across the whole domain, due to insignificant changes of SOA. In
360 summer, AOD_r increases in YRD and the adjacent area of Hubei, Hunan, and Jiangxi
361 province by up to 12%.

362 ARF represents the changes in the radiative flux due to aerosols. The off-line version
363 of the Shortwave Radiative Transfer Model For GCMs (RRTMG_SW) is used to calculate
364 the direct radiative effect of aerosols on shortwave radiation (Iacono et al., 2008). Generally,
365 fine aerosols exhibit cooling effects on the shortwave radiation in both winter and summer
366 over the entire domain as shown in Figure 6. This impact is much stronger in the areas



367 where AOD is high (Figure 5). The ARF at top of atmosphere (TOA) is highest in
368 Shandong in winter and coastal areas near Jiangsu province, which are about -12 W m^{-2}
369 and -9 W m^{-2} , respectively. In winter, no significant changes of ARF are observed in the
370 high regions of eastern China (Figure 6). This is likely attributed to an insignificant
371 contribution of SOA to $\text{PM}_{2.5}$ in winter compared to other components with cooling effects,
372 such as sulfate. In summer, SOA is an important component of $\text{PM}_{2.5}$ (20-60%), and the
373 effects of water partitioning on shortwave radiation is relatively stronger. An enhancement
374 of up to 15% in the cooling effects of ARF occurs near YRD region where AOD
375 significantly changes as well.

376 **4 Discussion**

377 Meteorological conditions and SOA precursors affect the impacts of water partitioning on
378 SOA. Figure 7 shows the effects of different factors on the daily maximum change of SOA
379 in Jinan and Nanjing, two representative cities in winter and summer, respectively. As
380 shown in Figure 7(a), the daily maximum elevation of SOA occurs when RH is greater than
381 70% in both cities. This is consistent with the previous study in the Southeast U.S. during
382 summer (Pankow et al., 2015). A clear correlation of the changes in SOA with SOA
383 concentration in Nanjing ($R=0.84$) during summer can be observed. However, this
384 correlation is relatively weak in Jinan ($R=0.44$) during winter. There is no strong
385 correlation between changes in SOA and temperature as shown in Figure 7(b), likely due
386 to the daily variation of SOA mass and composition. To better illustrate the dependency of
387 SOA on temperature and relative humidity, an offline calculation of SOA formation was
388 performed at Jinan and Nanjing when the daily maximum SOA increases occurred. We
389 assumed temperature (T) and water vapor mixing ratio (QV) to be within the range of $\bar{X} \pm$
390 σ , where \bar{X} and σ are the mean and standard deviation calculated based on WRF
391 prediction at each location. We chose 10 evenly distributed values for T and QV within the
392 range of $\bar{X} \pm \sigma$. The temperature dependence parameter of saturation vapor pressure (ΔH)
393 was also scaled by 0.2, 0.8, 1.4 and 2.0 separately for all the SVOCs. As shown in Figure



394 8, SOA indicates a negative correlation with temperature and a positive correlation with
395 RH in both cities. SOA is more sensitive to RH under cool conditions (JN) and to
396 temperature under hot conditions (NJ). An interesting finding is that significant increases
397 in SOA in the two cities occur during different time periods of the day. Water partitioning
398 tends to affect SOA in the afternoon and evening in Jinan, which mostly happens in the
399 early morning and at noon in Nanjing. The different timing is likely attributed to a
400 substantial increase in SOA precursors in the two cities. In Jinan, the most contributing
401 SVOCs are originated from toluene and xylenes oxidation, as well as oligomers formed by
402 their oxidation products in OPM. Possible emission sources include transportation,
403 petroleum refining, manufacturing, painting, etc. SOA increase in Nanjing is mostly
404 associated with biogenic sources including isoprene and monoterpenes.

405 Impacts of water partitioning into OPM and non-ideality of organic-water mixture on
406 SOA are opposite. Water partitioning alone increases SOA by ~20-60% in winter and ~20-
407 100% in summer (Figure S12). This is because that the molecular weight of water is quite
408 small and will reduce the molar averaged weight of OPM (\overline{MW}) in Eq 2 (Pankow et al.,
409 2015). The reduced \overline{MW} further increases $K_{p,i}$ promoting the mass transfer of SVOCs
410 from the gas phase to the OPM. On the other hand, by considering non-ideality of organic-
411 water mixture, activity coefficients of SVOCs are usually greater than 1.0 in this study,
412 leading to a decrease in $K_{p,i}$. As a result, the total SOA concentration is reduced by up to
413 ~10% in winter and ~30% in summer in the high regions (Figure S13). Overall, the final
414 impacts are the combined consequences of the two “processes”. In winter, the increase of
415 SOA caused by water partitioning is offset by the decrease of SOA due to the polarity of
416 SVOCs in most areas of the domain, resulting in no significant changes. In summer, effects
417 of water partitioning overcome that of SVOC polarity so as the total SOA loading increases.
418 This further leads to an enhanced attenuation of shortwave solar radiation and cooling of
419 the atmosphere.

420 **5 Conclusion**



421 The WRF/CMAQ model was used to investigate the impacts of water partitioning into
422 OPM and non-ideality of organic-water mixture on SOA formation over eastern China
423 during January and July of 2013. SOA is greatly enhanced in summer especially in YRD
424 and over Yellow Sea by up to 90% and 70% at the surface and the whole column,
425 respectively. No significant impacts on SOA are observed in winter. ALW_{org} is highly
426 correlated with the changes of SOA, with the ratio of ALW_{org} to SOA of 0.1-0.5 and 0.1-
427 0.6 at the surface where significant changes of SOA occur in winter and summer,
428 respectively. By using the modeled ALW_{org} , correlations between κ_{org} and O:C were
429 examined in 9 representative cities, showing significant spatial and seasonal variations.
430 The increases in SOA lead to 12% elevation of AOD and 15% enhancement in the cooling
431 effects of ARF in summer. The effects of water partitioning into OPM and non-ideality of
432 organic-water mixture on SOA were also examined separately. Since the activity
433 coefficients of SVOCs are mostly greater than 1.0 during the simulated episode, SOA
434 concentrations decrease when non-ideality effect is considered. Daily SOA concentration
435 decreases by up to ~10% in winter and ~30% in summer in the high regions. Water
436 partitioning alone increases SOA by ~20-60% in winter and ~20-100% in summer. It
437 should be noticed that the results shown in this study are the lower limit as the current
438 model tends to underestimate SOA. It is crucial to consider both effects in simulating SOA
439 formation under hot and humid conditions in CTMs.

440

441 *Data availability.* Data used in this manuscript can be provided upon request by e-mail to
442 the corresponding authors Qi Ying (qying@civil.tamu.edu), and Jianlin Hu
443 (jianlinhu@nuist.edu.cn).

444

445 *Author contributions.* J.L. and Q.Y. revised the model. J.L. performed the simulations.
446 Yan.Z., X.W., X.L. and Y.S. provided observations of OC and OA. J.L. and H.Z. processed
447 and analyzed the data. J.L., H.Z., Q.Y., J.H. and Z.W. discussed the results. J.L., Q.Y. and



448 J.H. contributed to writing and editing of the manuscript with comments from all the co-
449 authors.

450

451 *Competing interests.* The authors declare that they have no conflict of interest.

452

453 *Acknowledgments.* This project was partly supported by National Key R&D Program of
454 China (2018YFC0213802, Task #2), National Science Foundation of China (No. 41705102
455 and 41875149), and the Major Research Plan of National Social Science Foundation
456 (18ZDA052). The authors thank James F. Pankow for providing SOA module code. Jingyi
457 Li acknowledges support from the Startup Foundation for Introducing Talent of NUIST
458 grant no. 2243141701014, the Priority Academic Program Development of Jiangsu Higher
459 Education Institutions (PAPD), and Six Talent Peaks Project of Jiangsu Province.

460

461 **References**

- 462 Ansari, A. S., and Pandis, S. N.: Water Absorption by Secondary Organic Aerosol and Its Effect on
463 Inorganic Aerosol Behavior, *Environ. Sci. Technol.*, 34, 71-77, 10.1021/es990717q, 2000.
- 464 Asa-Awuku, A., Nenes, A., Gao, S., Flagan, R. C., and Seinfeld, J. H.: Water-soluble SOA from Alkene
465 ozonolysis: composition and droplet activation kinetics inferences from analysis of CCN activity, *Atmos.*
466 *Chem. Phys.*, 10, 1585-1597, 10.5194/acp-10-1585-2010, 2010.
- 467 Atkinson, R. W., Kang, S., Anderson, H. R., Mills, I. C., and Walton, H. A.: Epidemiological time series
468 studies of PM_{2.5} and daily mortality and hospital admissions: a systematic review and meta-analysis,
469 *Thorax*, 69, 660-665, 10.1136/thoraxjnl-2013-204492 %J Thorax, 2014.
- 470 Ayers, G. P.: Comment on regression analysis of air quality data, *Atmos. Environ.*, 35, 2423-2425,
471 [https://doi.org/10.1016/S1352-2310\(00\)00527-6](https://doi.org/10.1016/S1352-2310(00)00527-6), 2001.
- 472 Baek, J., Hu, Y., Odman, M. T., and Russell, A. G.: Modeling secondary organic aerosol in CMAQ using
473 multigenerational oxidation of semi-volatile organic compounds, 116, 10.1029/2011jd015911, 2011.
- 474 Bergström, R., Denier van der Gon, H. A. C., Prévôt, A. S. H., Yttri, K. E., and Simpson, D.: Modelling of
475 organic aerosols over Europe (2002‐2007) using a volatility basis set (VBS) framework:
476 application of different assumptions regarding the formation of secondary organic aerosol, *Atmos.*
477 *Chem. Phys.*, 12, 8499-8527, 10.5194/acp-12-8499-2012, 2012.
- 478 Bowman, F. M., and Melton, J. A.: Effect of activity coefficient models on predictions of secondary
479 organic aerosol partitioning, *J. Aerosol Sci.*, 35, 1415-1438,
480 <https://doi.org/10.1016/j.jaerosci.2004.07.001>, 2004.
- 481 Boylan, J. W., and Russell, A. G.: PM and light extinction model performance metrics, goals, and criteria
482 for three-dimensional air quality *Atmos. Environ.*, 40,
4946-4959,



- 483 <https://doi.org/10.1016/j.atmosenv.2005.09.087>, 2006.
- 484 Cappa, C. D., Lovejoy, E. R., and Ravishankara, A. R.: Evidence for liquid-like and nonideal behavior of
485 a mixture of organic aerosol components, *P. Natl. Acad. Sci. USA*, 105, 18687-18691,
486 10.1073/pnas.0802144105, 2008.
- 487 Chang, R. Y. W., Slowik, J. G., Shantz, N. C., Vlasenko, A., Liggio, J., Sjostedt, S. J., Leaitch, W. R., and
488 Abbatt, J. P. D.: The hygroscopicity parameter (κ) of ambient organic aerosol at a field site subject to
489 biogenic and anthropogenic influences: relationship to degree of aerosol oxidation, *Atmos. Chem.*
490 *Phys.*, 10, 5047-5064, 10.5194/acp-10-5047-2010, 2010.
- 491 Denjean, C., Formenti, P., Picquet-Varrault, B., Pangui, E., Zapf, P., Katrib, Y., Giorio, C., Tapparo, A.,
492 Monod, A., Temime-Roussel, B., Decorse, P., Mangeney, C., and Doussin, J. F.: Relating hygroscopicity
493 and optical properties to chemical composition and structure of secondary organic aerosol particles
494 generated from the ozonolysis of α -pinene, *Atmos. Chem. Phys.*, 15, 3339-3358, 10.5194/acp-15-
495 3339-2015, 2015.
- 496 Donahue, N. M., Robinson, A. L., Stanier, C. O., and Pandis, S. N.: Coupled partitioning, dilution, and
497 chemical aging of semivolatile organics, *Environ. Sci. Technol.*, 40, 02635-02643, 10.1021/es052297c,
498 2006.
- 499 Duplissy, J., DeCarlo, P. F., Dommen, J., Alfarra, M. R., Metzger, A., Barmapadimos, I., Prevot, A. S. H.,
500 Weingartner, E., Tritscher, T., Gysel, M., Aiken, A. C., Jimenez, J. L., Canagaratna, M. R., Worsnop, D. R.,
501 Collins, D. R., Tomlinson, J., and Baltensperger, U.: Relating hygroscopicity and composition of organic
502 aerosol particulate matter, *Atmos. Chem. Phys.*, 11, 1155-1165, 10.5194/acp-11-1155-2011, 2011.
- 503 Ehn, M., Thornton, J. A., Kleist, E., Sipilä, M., Junninen, H., Pullinen, I., Springer, M., Rubach, F., Tillmann,
504 R., Lee, B., Lopez-Hilfiker, F., Andres, S., Acir, I.-H., Rissanen, M., Jokinen, T., Schobesberger, S.,
505 Kangasluoma, J., Kontkanen, J., Nieminen, T., Kurtén, T., Nielsen, L. B., Jørgensen, S., Kjaergaard, H. G.,
506 Canagaratna, M., Maso, M. D., Berndt, T., Petäjä, T., Wahner, A., Kerminen, V.-M., Kulmala, M., Worsnop,
507 D. R., Wildt, J., and Mentel, T. F.: A large source of low-volatility secondary organic aerosol, *Nature*,
508 506, 476, 10.1038/nature13032, 2014.
- 509 Ervens, B., Turpin, B. J., and Weber, R. J.: Secondary organic aerosol formation in cloud droplets and
510 aqueous particles (aqSOA): a review of laboratory, field and model studies, *Atmos. Chem. Phys.*, 11,
511 11069-11102, 10.5194/acp-11-11069-2011, 2011.
- 512 Feng, S., Gao, D., Liao, F., Zhou, F., and Wang, X.: The health effects of ambient PM_{2.5} and potential
513 mechanisms, *Ecotox. Environ. Safe.*, 128, 67-74, <https://doi.org/10.1016/j.ecoenv.2016.01.030>, 2016.
- 514 Fredenslund, A., Jones, R. L., and Prausnitz, J. M.: Group-contribution estimation of activity coefficients
515 in nonideal liquid mixtures, 21, 1086-1099, doi:10.1002/aic.690210607, 1975.
- 516 Fu, H., and Chen, J.: Formation, features and controlling strategies of severe haze-fog pollutions in
517 China, *Sci. Total Environ.*, 578, 121-138, <https://doi.org/10.1016/j.scitotenv.2016.10.201>, 2017.
- 518 Gentner, D. R., Jathar, S. H., Gordon, T. D., Bahreini, R., Day, D. A., El Haddad, I., Hayes, P. L., Pieber, S.
519 M., Platt, S. M., de Gouw, J., Goldstein, A. H., Harley, R. A., Jimenez, J. L., Prévôt, A. S. H., and Robinson,
520 A. L.: Review of Urban Secondary Organic Aerosol Formation from Gasoline and Diesel Motor Vehicle
521 Emissions, *Environ. Sci. Technol.*, 51, 1074-1093, 10.1021/acs.est.6b04509, 2017.
- 522 Guo, H., Xu, L., Bougiatioti, A., Cerully, K. M., Capps, S. L., Hite Jr, J. R., Carlton, A. G., Lee, S. H., Bergin,
523 M. H., Ng, N. L., Nenes, A., and Weber, R. J.: Fine-particle water and pH in the southeastern United



- 524 States, *Atmos. Chem. Phys.*, 15, 5211–5228, 10.5194/acp-15-5211-2015, 2015.
- 525 Guo, S., Hu, M., Zamora, M. L., Peng, J., Shang, D., Zheng, J., Du, Z., Wu, Z., Shao, M., Zeng, L., Molina,
526 M. J., and Zhang, R.: Elucidating severe urban haze formation in China, *P. Natl. Acad. Sci. USA*, 111,
527 17373–17378, 10.1073/pnas.1419604111 2014.
- 528 Hatzianastassiou, N., Matsoukas, C., Drakakis, E., Stackhouse Jr, P. W., Koepke, P., Fotiadis, A., Pavlakis,
529 K. G., and Vardavas, I.: The direct effect of aerosols on solar radiation based on satellite observations,
530 reanalysis datasets, and spectral aerosol optical properties from Global Aerosol Data Set (GADS),
531 *Atmos. Chem. Phys.*, 7, 2585–2599, 10.5194/acp-7-2585-2007, 2007.
- 532 Hayes, P. L., Carlton, A. G., Baker, K. R., Ahmadov, R., Washenfelder, R. A., Alvarez, S., Rappenglück, B.,
533 Gilman, J. B., Kuster, W. C., de Gouw, J. A., Zotter, P., Prévôt, A. S. H., Szidat, S., Kleindienst, T. E.,
534 Offenberg, J. H., Ma, P. K., and Jimenez, J. L.: Modeling the formation and aging of secondary organic
535 aerosols in Los Angeles during CalNex 2010, *Atmos. Chem. Phys.*, 15, 5773–5801, 10.5194/acp-15-
536 5773-2015, 2015.
- 537 He, Q., Zhang, M., and Huang, B.: Spatio-temporal variation and impact factors analysis of satellite-
538 based aerosol optical depth over China from 2002 to 2015, *Atmos. Environ.*, 129, 79–90,
539 <https://doi.org/10.1016/j.atmosenv.2016.01.002>, 2016.
- 540 He, Q., Gu, Y., and Zhang, M.: Spatiotemporal patterns of aerosol optical depth throughout China from
541 2003 to 2016, *Sci. Total Environ.*, 653, 23–35, <https://doi.org/10.1016/j.scitotenv.2018.10.307>, 2019.
- 542 Heald, C. L., Jacob, D. J., Turquety, S., Hudman, R. C., Weber, R. J., Sullivan, A. P., Peltier, R. E., Atlas, E.
543 L., de Gouw, J. A., Warneke, C., Holloway, J. S., Neuman, J. A., Flocke, F. M., and Seinfeld, J. H.:
544 Concentrations and sources of organic carbon aerosols in the free troposphere over North America,
545 *J. Geophys. Res.*, 111, D23S47, 10.1029/2006jd007705, 2006.
- 546 Healy, R. M., Temime, B., Kuprovskite, K., and Wenger, J. C.: Effect of Relative Humidity on Gas/Particle
547 Partitioning and Aerosol Mass Yield in the Photooxidation of p-Xylene, *Environ. Sci. Technol.*, 43,
548 1884–1889, 10.1021/es802404z, 2009.
- 549 Hegerl, G. C., Black, E., Allan, R. P., Ingram, W. J., Polson, D., Trenberth, K. E., Chadwick, R. S., Arkin, P.
550 A., Sarojini, B. B., Becker, A., Dai, A., Durack, P. J., Easterling, D., Fowler, H. J., Kendon, E. J., Huffman, G.
551 J., Liu, C., Marsh, R., New, M., Osborn, T. J., Skliris, N., Stott, P. A., Vidale, P.-L., Wjiffels, S. E., Wilcox, L.
552 J., Willett, K. M., and Zhang, X.: CHALLENGES IN QUANTIFYING CHANGES IN THE GLOBAL WATER
553 CYCLE, *Bull. Am. Meteorol. Soc.*, 96, 1097–1116, 2015.
- 554 Hong, J., Xu, H., Tan, H., Yin, C., Hao, L., Li, F., Cai, M., Deng, X., Wang, N., Su, H., Cheng, Y., Wang, L.,
555 Petäjä, T., and Kerminen, V. M.: Mixing state and particle hygroscopicity of organic-dominated aerosols
556 over the Pearl River Delta region in China, *Atmos. Chem. Phys.*, 18, 14079–14094, 10.5194/acp-18-
557 14079-2018, 2018.
- 558 Hu, J., Chen, J., Ying, Q., and Zhang, H.: One-year simulation of ozone and particulate matter in China
559 using WRF/CMAQ modeling system, *Atmos. Chem. Phys.*, 16, 10333–10350, 10.5194/acp-16-10333-
560 2016, 2016.
- 561 Hu, J., Wang, P., Ying, Q., Zhang, H., Chen, J., Ge, X., Li, X., Jiang, J., Wang, S., Zhang, J., Zhao, Y., and
562 Zhang, Y.: Modeling biogenic and anthropogenic secondary organic aerosol in China, *Atmos. Chem.
563 Phys.*, 17, 77–92, 10.5194/acp-17-77-2017, 2017.
- 564 Huang, R.-J., Zhang, Y., Bozzetti, C., Ho, K.-F., Cao, J.-J., Han, Y., Daellenbach, K. R., Slowik, J. G., Platt,



- 565 S. M., Canonaco, F., Zotter, P., Wolf, R., Pieber, S. M., Bruns, E. A., Crippa, M., Ciarelli, G., Piazzalunga,
566 A., Schwikowski, M., Abbaszade, G., Schnelle-Kreis, J., Zimmermann, R., An, Z., Szidat, S., Baltensperger,
567 U., Haddad, I. E., and Prévôt, A. S. H.: High secondary aerosol contribution to particulate pollution
568 during haze events in China, *Nature*, 514, 218, [10.1038/nature13774](https://doi.org/10.1038/nature13774), 2014.
- 569 Huang, W., Saathoff, H., Shen, X., Ramisetty, R., Leisner, T., and Mohr, C.: Chemical Characterization of
570 Highly Functionalized Organonitrates Contributing to Night-Time Organic Aerosol Mass Loadings and
571 Particle Growth, *Environ. Sci. Technol.*, 53, 1165-1174, [10.1021/acs.est.8b05826](https://doi.org/10.1021/acs.est.8b05826), 2019.
- 572 Iacono, M. J., Delamere, J. S., Mlawer, E. J., Shephard, M. W., Clough, S. A., and Collins, W. D.: Radiative
573 forcing by long-lived greenhouse gases: Calculations with the AER radiative transfer models, *J.*
574 *Geophys. Res.*, 113, D13103, [10.1029/2008jd009944](https://doi.org/10.1029/2008jd009944), 2008.
- 575 Jathar, S. H., Mahmud, A., Barsanti, K. C., Asher, W. E., Pankow, J. F., and Kleeman, M. J.: Water uptake
576 by organic aerosol and its influence on gas/particle partitioning of secondary organic aerosol in the
577 United States, *Atmos. Environ.*, 129, 142-154, <https://doi.org/10.1016/j.atmosenv.2016.01.001>, 2016.
- 578 Jiang, F., Liu, Q., Huang, X., Wang, T., Zhuang, B., and Xie, M.: Regional modeling of secondary organic
579 aerosol over China using WRF/Chem, *J. Aerosol Sci.*, 43, 57-73,
580 <https://doi.org/10.1016/j.jaerosci.2011.09.003>, 2012.
- 581 Jokinen, T., Berndt, T., Makkonen, R., Kerminen, V.-M., Junninen, H., Paasonen, P., Stratmann, F.,
582 Herrmann, H., Guenther, A. B., Worsnop, D. R., Kulmala, M., Ehn, M., and Sipilä, M.: Production of
583 extremely low volatile organic compounds from biogenic emissions: Measured yields and atmospheric
584 implications, 112, 7123-7128, [10.1073/pnas.1423977112](https://doi.org/10.1073/pnas.1423977112) %J Proceedings of the National Academy of
585 Sciences, 2015.
- 586 Kim, Y., Sartelet, K., and Couvidat, F.: Modeling the effect of non-ideality, dynamic mass transfer and
587 viscosity on SOA formation in a 3-D air quality model, *Atmos. Chem. Phys.*, 19, 1241-1261,
588 [10.5194/acp-19-1241-2019](https://doi.org/10.5194/acp-19-1241-2019), 2019.
- 589 Kurokawa, J., Ohara, T., Morikawa, T., Hanayama, S., Janssens-Maenhout, G., Fukui, T., Kawashima, K.,
590 and Akimoto, H.: Emissions of air pollutants and greenhouse gases over Asian regions during 2000–
591 2008: Regional Emission inventory in ASia (REAS) version 2, *Atmos. Chem. Phys.*, 13, 11019-11058,
592 [10.5194/acp-13-11019-2013](https://doi.org/10.5194/acp-13-11019-2013), 2013.
- 593 Lambe, A. T., Onasch, T. B., Massoli, P., Croasdale, D. R., Wright, J. P., Ahern, A. T., Williams, L. R.,
594 Worsnop, D. R., Brune, W. H., and Davidovits, P.: Laboratory studies of the chemical composition and
595 cloud condensation nuclei (CCN) activity of secondary organic aerosol (SOA) and oxidized primary
596 organic aerosol (OPOA), *Atmos. Chem. Phys.*, 11, 8913-8928, [10.5194/acp-11-8913-2011](https://doi.org/10.5194/acp-11-8913-2011), 2011.
- 597 Levy, R. C., Remer, L. A., Kleidman, R. G., Mattoo, S., Ichoku, C., Kahn, R., and Eck, T. F.: Global evaluation
598 of the Collection 5 MODIS dark-target aerosol products over land, *Atmos. Chem. Phys.*, 10, 10399-
599 10420, [10.5194/acp-10-10399-2010](https://doi.org/10.5194/acp-10-10399-2010), 2010.
- 600 Li, J., Cleveland, M., Ziemba, L. D., Griffin, R. J., Barsanti, K. C., Pankow, J. F., and Ying, Q.: Modeling
601 regional secondary organic aerosol using the Master Chemical Mechanism, *Atmos. Environ.*, 102, 52-
602 61, <https://doi.org/10.1016/j.atmosenv.2014.11.054>, 2015.
- 603 Li, J., Zhang, M., Wu, F., Sun, Y., and Tang, G.: Assessment of the impacts of aromatic VOC emissions
604 and yields of SOA on SOA concentrations with the air quality model RAMS-CMAQ, *Atmos. Environ.*,
605 158, 105-115, <https://doi.org/10.1016/j.atmosenv.2017.03.035>, 2017a.



- 606 Li, M., Zhang, Q., Streets, D. G., He, K. B., Cheng, Y. F., Emmons, L. K., Huo, H., Kang, S. C., Lu, Z., Shao,
607 M., Su, H., Yu, X., and Zhang, Y.: Mapping Asian anthropogenic emissions of non-methane volatile
608 organic compounds to multiple chemical mechanisms, *Atmos. Chem. Phys.*, 14, 5617-5638,
609 10.5194/acp-14-5617-2014, 2014.
- 610 Li, X., Song, S., Zhou, W., Hao, J., Worsnop, D. R., and Jiang, J.: Interactions between aerosol organic
611 components and liquid water content during haze episodes in Beijing, *Atmos. Chem. Phys.*, 19, 12163-
612 12174, 10.5194/acp-19-12163-2019, 2019.
- 613 Li, Y. J., Sun, Y., Zhang, Q., Li, X., Li, M., Zhou, Z., and Chan, C. K.: Real-time chemical characterization
614 of atmospheric particulate matter in China: A review, *Atmos. Environ.*, 158, 270-304,
615 <https://doi.org/10.1016/j.atmosenv.2017.02.027>, 2017b.
- 616 Lin, J., An, J., Qu, Y., Chen, Y., Li, Y., Tang, Y., Wang, F., and Xiang, W.: Local and distant source
617 contributions to secondary organic aerosol in the Beijing urban area in summer, *Atmos. Environ.*, 124,
618 176-185, <https://doi.org/10.1016/j.atmosenv.2015.08.098>, 2016.
- 619 Liu, F., Zhang, Q., Tong, D., Zheng, B., Li, M., Huo, H., and He, K. B.: High-resolution inventory of
620 technologies, activities, and emissions of coal-fired power plants in China from 1990 to 2010, *Atmos.*
621 *Chem. Phys.*, 15, 13299-13317, 10.5194/acp-15-13299-2015, 2015.
- 622 Liu, X.-H., Zhang, Y., Cheng, S.-H., Xing, J., Zhang, Q., Streets, D. G., Jang, C., Wang, W.-X., and Hao,
623 J.-M.: Understanding of regional air pollution over China using CMAQ, part I performance evaluation
624 and seasonal variation, *Atmos. Environ.*, 44, 2415-2426,
625 <https://doi.org/10.1016/j.atmosenv.2010.03.035>, 2010.
- 626 Liu, X., and Wang, J.: How important is organic aerosol hygroscopicity to aerosol indirect forcing?,
627 *Environ. Res. Lett.*, 5, 044010, 10.1088/1748-9326/5/4/044010, 2010.
- 628 Liu, X. H., Zhu, Y. J., Zheng, M., Gao, H. W., and Yao, X. H.: Production and growth of new particles
629 during two cruise campaigns in the marginal seas of China, *Atmos. Chem. Phys.*, 14, 7941-7951,
630 10.5194/acp-14-7941-2014, 2014.
- 631 Luo, Y. X., Zheng, X. B., Zhao, T. L., and Chen, J.: A climatology of aerosol optical depth over China
632 from recent 10 years of MODIS remote sensing data, *Int. J. Climatol.*, 34, 863-870, 10.1002/joc.3728,
633 2014.
- 634 Malm, W. C., Sisler, J. F., Huffman, D., Eldred, R. A., and Cahill, T. A.: Spatial and seasonal trends in
635 particle concentration and optical extinction in the United States, *J. Geophys. Res.*, 99, 1347-1370,
636 doi:10.1029/93JD02916, 1994.
- 637 Man, H., Zhu, Y., Ji, F., Yao, X., Lau, N. T., Li, Y., Lee, B. P., and Chan, C. K.: Comparison of Daytime and
638 Nighttime New Particle Growth at the HKUST Supersite in Hong Kong, *Environ. Sci. Technol.*, 49, 7170-
639 7178, 10.1021/acs.est.5b02143, 2015.
- 640 Massoli, P., Lambe, A. T., Ahern, A. T., Williams, L. R., Ehn, M., Mikkilä, J., Canagaratna, M. R., Brune, W.
641 H., Onasch, T. B., Jayne, J. T., Petäjä, T., Kulmala, M., Laaksonen, A., Kolb, C. E., Davidovits, P., and
642 Worsnop, D. R.: Relationship between aerosol oxidation level and hygroscopic properties of laboratory
643 generated secondary organic aerosol (SOA) particles, *Geophys. Res. Lett.*, 37, 1-5,
644 doi:10.1029/2010GL045258, 2010.
- 645 Meyer, N. K., Duplissy, J., Gysel, M., Metzger, A., Dommen, J., Weingartner, E., Alfarra, M. R., Prevot, A.
646 S. H., Fletcher, C., Good, N., McFiggans, G., Jonsson, Å. M., Hallquist, M., Baltensperger, U., and Ristovski,



- 647 Z. D.: Analysis of the hygroscopic and volatile properties of ammonium sulphate seeded and unseeded
648 SOA particles, *Atmos. Chem. Phys.*, 9, 721-732, 10.5194/acp-9-721-2009, 2009.
- 649 Odum, J. R., Hoffmann, T., Bowman, F., Collins, D., Flagan, R. C., and Seinfeld, J. H.: Gas/Particle
650 Partitioning and Secondary Organic Aerosol Yields, *Environ. Sci. Technol.*, 30, 2580-2585,
651 10.1021/es950943+, 1996.
- 652 Pankow, J. F.: An absorption model of gas/particle partitioning of organic compounds in the
653 atmosphere, *Atmos. Environ.*, 28, 185-188, [https://doi.org/10.1016/1352-2310\(94\)90093-0](https://doi.org/10.1016/1352-2310(94)90093-0), 1994.
- 654 Pankow, J. F., Marks, M. C., Barsanti, K. C., Mahmud, A., Asher, W. E., Li, J., Ying, Q., Jathar, S. H., and
655 Kleeman, M. J.: Molecular view modeling of atmospheric organic particulate matter: Incorporating
656 molecular structure and co-condensation of water, *Atmos. Environ.*, 122, 400-408,
657 <https://doi.org/10.1016/j.atmosenv.2015.10.001>, 2015.
- 658 Peter, T., Marcolli, C., Spichtinger, P., Corti, T., Baker, M. B., and Koop, T.: When Dry Air Is Too Humid,
659 *Science*, 314, 1399-1402, 10.1126/science.1135199, 2006.
- 660 Petters, M. D., and Kreidenweis, S. M.: A single parameter representation of hygroscopic growth and
661 cloud condensation nucleus activity, *Atmos. Chem. Phys.*, 7, 1961-1971, 10.5194/acp-7-1961-2007,
662 2007.
- 663 Polichetti, G., Cocco, S., Spinali, A., Trimarco, V., and Nunziata, A.: Effects of particulate matter (PM10,
664 PM2.5 and PM1) on the cardiovascular system, *Toxicology*, 261, 1-8,
665 <https://doi.org/10.1016/j.tox.2009.04.035>, 2009.
- 666 Poulain, L., Wu, Z., Petters, M. D., Wex, H., Hallbauer, E., Wehner, B., Massling, A., Kreidenweis, S. M.,
667 and Stratmann, F.: Towards closing the gap between hygroscopic growth and CCN activation for
668 secondary organic aerosols – Part 3: Influence of the chemical composition on the hygroscopic
669 properties and volatile fractions of aerosols, *Atmos. Chem. Phys.*, 10, 3775-3785, 10.5194/acp-10-
670 3775-2010, 2010.
- 671 Prisle, N. L., Engelhart, G. J., Bilde, M., and Donahue, N. M.: Humidity influence on gas-particle phase
672 partitioning of α -pinene + O₃ secondary organic aerosol, *Geophys. Res. Lett.*, 37, 1-5,
673 10.1029/2009gl041402, 2010.
- 674 Pye, H. O. T., Murphy, B. N., Xu, L., Ng, N. L., Carlton, A. G., Guo, H., Weber, R., Vasilakos, P., Appel, K.
675 W., Budisulistiorini, S. H., Surratt, J. D., Nenes, A., Hu, W., Jimenez, J. L., Isaacman-VanWertz, G., Misztal,
676 P. K., and Goldstein, A. H.: On the implications of aerosol liquid water and phase separation for organic
677 aerosol mass, *Atmos. Chem. Phys.*, 17, 343-369, 10.5194/acp-17-343-2017, 2017.
- 678 Quaas, J., Boucher, O., Bellouin, N., and Kinne, S.: Satellite-based estimate of the direct and indirect
679 aerosol climate forcing, *J. Geophys. Res.*, 113, D505204, doi:10.1029/2007JD008962, 2008.
- 680 Ramanathan, V., Crutzen, P. J., Kiehl, J. T., and Rosenfeld, D.: Aerosols, Climate, and the Hydrological
681 Cycle, *Science*, 294, 2119-2124, 10.1126/science.1064034, 2001.
- 682 Rickards, A. M. J., Miles, R. E. H., Davies, J. F., Marshall, F. H., and Reid, J. P.: Measurements of the
683 Sensitivity of Aerosol Hygroscopicity and the κ Parameter to the O/C Ratio, *J. Phys. Chem. A*, 117,
684 14120-14131, 10.1021/jp407991n, 2013.
- 685 Rosenfeld, D., Lohmann, U., Raga, G. B., O'Dowd, C. D., Kulmala, M., Fuzzi, S., Reissell, A., and Andreae,
686 M. O.: Flood or Drought: How Do Aerosols Affect Precipitation?, *Science*, 321, 1309-1313,
687 10.1126/science.1160606, 2008.



- 688 Seinfeld, J. H., Erdakos, G. B., Asher, W. E., and Pankow, J. F.: Modeling the Formation of Secondary
689 Organic Aerosol (SOA). 2. The Predicted Effects of Relative Humidity on Aerosol Formation in the α -
690 Pinene-, β -Pinene-, Sabinene-, Δ 3-Carene-, and Cyclohexene-Ozone Systems, *Environ. Sci. Technol.*,
691 35, 1806-1817, 10.1021/es001765+, 2001.
- 692 Shrivastava, M., Cappa, C. D., Fan, J., Goldstein, A. H., Guenther, A. B., Jimenez, J. L., Kuang, C., Laskin,
693 A., Martin, S. T., Ng, N. L., Petaja, T., Pierce, J. R., Rasch, P. J., Roldin, P., Seinfeld, J. H., Shilling, J., Smith,
694 J. N., Thornton, J. A., Volkamer, R., Wang, J., Worsnop, D. R., Zaveri, R. A., Zelenyuk, A., and Zhang, Q.:
695 Recent advances in understanding secondary organic aerosol: Implications for global climate forcing,
696 *Rev. Geophys.*, 55, 509-559, doi:10.1002/2016RG000540, 2017.
- 697 Simon, H., and Bhave, P. V.: Simulating the Degree of Oxidation in Atmospheric Organic Particles,
698 *Environ. Sci. Technol.*, 46, 331-339, 10.1021/es202361w, 2012.
- 699 Slowik, J. G., Stroud, C., Bottenheim, J. W., Brickell, P. C., Chang, R. Y. W., Liggio, J., Makar, P. A., Martin,
700 R. V., Moran, M. D., Shantz, N. C., Sjostedt, S. J., van Donkelaar, A., Vlasenko, A., Wiebe, H. A., Xia, A.
701 G., Zhang, J., Leaitch, W. R., and Abbatt, J. P. D.: Characterization of a large biogenic secondary organic
702 aerosol event from eastern Canadian forests, *Atmos. Chem. Phys.*, 10, 2825-2845, 10.5194/acp-10-
703 2825-2010, 2010.
- 704 Spracklen, D. V., Jimenez, J. L., Carslaw, K. S., Worsnop, D. R., Evans, M. J., Mann, G. W., Zhang, Q.,
705 Canagaratna, M. R., Allan, J., Coe, H., McFiggans, G., Rap, A., and Forster, P.: Aerosol mass spectrometer
706 constraint on the global secondary organic aerosol budget, *Atmos. Chem. Phys.*, 11, 12109-12136,
707 10.5194/acp-11-12109-2011, 2011.
- 708 Sun, J., Liang, M., Shi, Z., Shen, F., Li, J., Huang, L., Ge, X., Chen, Q., Sun, Y., Zhang, Y., Chang, Y., Ji, D.,
709 Ying, Q., Zhang, H., Kota, S. H., and Hu, J.: Investigating the PM_{2.5} mass concentration growth
710 processes during 2013–2016 in Beijing and Shanghai, *Chemosphere*, 221, 452-463,
711 <https://doi.org/10.1016/j.chemosphere.2018.12.200>, 2019.
- 712 Tritscher, T., Dommen, J., DeCarlo, P. F., Gysel, M., Barmet, P. B., Praplan, A. P., Weingartner, E., Prévôt,
713 A. S. H., Riipinen, I., Donahue, N. M., and Baltensperger, U.: Volatility and hygroscopicity of aging
714 secondary organic aerosol in a smog chamber, *Atmos. Chem. Phys.*, 11, 11477-11496, 10.5194/acp-
715 11-11477-2011, 2011a.
- 716 Tritscher, T., Jurányi, Z., Martin, M., Chirico, R., Gysel, M., Heringa, M. F., DeCarlo, P. F., Sierau, B., Prévôt,
717 A. S. H., Weingartner, E., and Baltensperger, U.: Changes of hygroscopicity and morphology during
718 ageing of diesel soot, *Environ. Res. Lett.*, 6, 1-10, 10.1088/1748-9326/6/3/034026, 2011b.
- 719 Varutbangkul, V., Brechtel, F. J., Bahreini, R., Ng, N. L., Keywood, M. D., Kroll, J. H., Flagan, R. C., Seinfeld,
720 J. H., Lee, A., and Goldstein, A. H.: Hygroscopicity of secondary organic aerosols formed by oxidation
721 of cycloalkenes, monoterpenes, sesquiterpenes, and related compounds, *Atmos. Chem. Phys.*, 6, 2367-
722 2388, 10.5194/acp-6-2367-2006, 2006.
- 723 Wang, K., Zhang, Y., Jang, C., Phillips, S., and Wang, B.: Modeling intercontinental air pollution transport
724 over the trans-Pacific region in 2001 using the Community Multiscale Air Quality modeling system, *J.*
725 *Geophys. Res.*, 114, D04307, doi:10.1029/2008JD010807, 2009.
- 726 Wang, S., Xing, J., Chatani, S., Hao, J., Klimont, Z., Cofala, J., and Amann, M.: Verification of
727 anthropogenic emissions of China by satellite and ground observations, *Atmos. Environ.*, 45, 6347-
728 6358, <https://doi.org/10.1016/j.atmosenv.2011.08.054>, 2011.



- 729 Wang, X., Ye, X., Chen, H., Chen, J., Yang, X., and Gross, D. S.: Online hygroscopicity and chemical
730 measurement of urban aerosol in Shanghai, China, *Atmos. Environ.*, 95, 318-326,
731 <https://doi.org/10.1016/j.atmosenv.2014.06.051>, 2014.
- 732 Wiedensohler, A., Cheng, Y. F., Nowak, A., Wehner, B., Achtert, P., Berghof, M., Birmili, W., Wu, Z. J., Hu,
733 M., Zhu, T., Takegawa, N., Kita, K., Kondo, Y., Lou, S. R., Hofzumahaus, A., Holland, F., Wahner, A.,
734 Gunthe, S. S., Rose, D., Su, H., and Pöschl, U.: Rapid aerosol particle growth and increase of cloud
735 condensation nucleus activity by secondary aerosol formation and condensation: A case study for
736 regional air pollution in northeastern China, *J. Geophys. Res.*, 114, D00G08, doi:10.1029/2008JD010884,
737 2009.
- 738 Wiedinmyer, C., Akagi, S. K., Yokelson, R. J., Emmons, L. K., Al-Saadi, J. A., Orlando, J. J., and Soja, A. J.:
739 The Fire INventory from NCAR (FINN): a high resolution global model to estimate the emissions from
740 open burning, *Geosci. Model Dev.*, 4, 625-641, 10.5194/gmd-4-625-2011, 2011.
- 741 Woody, M. C., Baker, K. R., Hayes, P. L., Jimenez, J. L., Koo, B., and Pye, H. O. T.: Understanding sources
742 of organic aerosol during CalNex-2010 using the CMAQ-VBS, *Atmos. Chem. Phys.*, 16, 4081-4100,
743 10.5194/acp-16-4081-2016, 2016.
- 744 Xing, Y.-F., Xu, Y.-H., Shi, M.-H., and Lian, Y.-X.: The impact of PM_{2.5} on the human respiratory system,
745 *J. Thorac. Dis.*, 8, E69-E74, 10.3978/j.issn.2072-1439.2016.01.19, 2016.
- 746 Yang, Y., Liao, H., and Lou, S.: Increase in winter haze over eastern China in recent decades: Roles of
747 variations in meteorological parameters and anthropogenic emissions, *J. Geophys. Res.*, 121, 13,050-
748 013,065, 10.1002/2016jd025136, 2016.
- 749 Ying, Q., Cureño, I. V., Chen, G., Ali, S., Zhang, H., Malloy, M., Bravo, H. A., and Sosa, R.: Impacts of
750 Stabilized Criegee Intermediates, surface uptake processes and higher aromatic secondary organic
751 aerosol yields on predicted PM_{2.5} concentrations in the Mexico City Metropolitan Zone, *Atmos.*
752 *Environ.*, 94, 438-447, <https://doi.org/10.1016/j.atmosenv.2014.05.056>, 2014.
- 753 Ying, Q., Li, J., and Kota, S. H.: Significant Contributions of Isoprene to Summertime Secondary Organic
754 Aerosol in Eastern United States, *Environ. Sci. Technol.*, 49, 7834-7842, 10.1021/acs.est.5b02514, 2015.
- 755 Yue, D. L., Hu, M., Zhang, R. Y., Wu, Z. J., Su, H., Wang, Z. B., Peng, J. F., He, L. Y., Huang, X. F., Gong,
756 Y. G., and Wiedensohler, A.: Potential contribution of new particle formation to cloud condensation
757 nuclei in Beijing, *Atmos. Environ.*, 45, 6070-6077, <https://doi.org/10.1016/j.atmosenv.2011.07.037>,
758 2011.
- 759 Zhang, H., Hu, J., Kleeman, M., and Ying, Q.: Source apportionment of sulfate and nitrate particulate
760 matter in the Eastern United States and effectiveness of emission control programs, *Sci. Total Environ.*,
761 490, 171-181, <https://doi.org/10.1016/j.scitotenv.2014.04.064>, 2014.
- 762 Zhang, Q., Streets, D. G., Carmichael, G. R., He, K. B., Huo, H., Kannari, A., Klimont, Z., Park, I. S., Reddy,
763 S., Fu, J. S., Chen, D., Duan, L., Lei, Y., Wang, L. T., and Yao, Z. L.: Asian emissions in 2006 for the NASA
764 INTEX-B mission, *Atmos. Chem. Phys.*, 9, 5131-5153, 10.5194/acp-9-5131-2009, 2009.
- 765 Zhang, X. Y., Sun, J. Y., Lin, W. L., Gong, S. L., Shen, X. J., and Yang, S.: Characterization of new particle
766 and secondary aerosol formation during summertime in Beijing, China *Tellus B*, 63, 382-394,
767 10.1111/j.1600-0889.2011.00533.x, 2011.
- 768 Zhao, B., Wang, S., Donahue, N. M., Jathar, S. H., Huang, X., Wu, W., Hao, J., and Robinson, A. L.:
769 Quantifying the effect of organic aerosol aging and intermediate-volatility emissions on regional-scale



770 aerosol pollution in China, *Sci. Rep.*, 6, 28815, 10.1038/srep28815, 2016a.
771 Zhao, D. F., Buchholz, A., Kortner, B., Schlag, P., Rubach, F., Fuchs, H., Kiendler-Scharr, A., Tillmann, R.,
772 Wahner, A., Watne, Å. K., Hallquist, M., Flores, J. M., Rudich, Y., Kristensen, K., Hansen, A. M. K., Glasius,
773 M., Kourtchev, I., Kalberer, M., and Mentel, T. F.: Cloud condensation nuclei activity, droplet growth
774 kinetics, and hygroscopicity of biogenic and anthropogenic secondary organic aerosol (SOA), *Atmos.*
775 *Chem. Phys.*, 16, 1105-1121, 10.5194/acp-16-1105-2016, 2016b.
776 Zheng, B., Huo, H., Zhang, Q., Yao, Z. L., Wang, X. T., Yang, X. F., Liu, H., and He, K. B.: High-resolution
777 mapping of vehicle emissions in China in 2008, *Atmos. Chem. Phys.*, 14, 9787-9805, 10.5194/acp-14-
778 9787-2014, 2014.
779



Table 1. Statistical analysis of modeled temperature (K) and relative humidity (%) of January and July at the monitoring sites in different geographical areas as shown in Figure S1.

	Northeast		NCP		Northwest		YRD		Central		Sichuan Basin		PRD		Southwest		
	Jan	Jul	Jan	Jul	Jan	Jul	Jan	Jul	Jan	Jul	Jan	Jul	Jan	Jul	Jan	Jul	
Temperature (K)	Obs	256.7	296.4	264.4	297.9	268.1	294.0	277.8	303.6	276.1	301.8	276.9	296.6	290.3	301.1	282.1	294.6
	Pred	251.6	296.5	261.3	298.9	268.5	295.0	278.5	302.8	276.3	301.5	274.5	294.0	289.4	300.2	278.4	291.1
	MB	-5.1	-0.1	-3.1	1.3	0.48	1.0	0.7	-0.8	-0.8	0.2	-0.3	-2.5	-2.6	-0.8	-3.7	-3.5
	GE	6.3	4.4	5.1	5.1	6.1	5.4	3.6	4.2	4.5	4.4	6.7	5.4	3.5	2.7	6.1	4.4
	Num	10101	11298	15072	16820	11475	12830	6835	7620	21210	23809	13573	15192	7017	7715	12088	13590
Relative Humidity (%)	Obs	77.9	80.4	74.9	72.4	61.0	70.8	79.3	69.5	76.9	71.2	69.5	74.2	76.0	80.8	69.6	78.7
	Pred	85.3	73.4	78.4	58.1	48.7	56.1	73.6	73.0	64.5	70.3	57.8	78.4	75.2	84.5	78.0	87.0
	MB	7.4	-7.0	3.5	-14.3	-12.3	-14.6	-5.6	3.4	-12.4	-0.9	-11.6	4.2	-0.8	3.7	8.4	8.2
	GE	12.4	19.2	16.2	22.7	21.3	22.6	17.6	17.8	20.8	17.9	25.5	17.2	15.0	13.8	20.6	16.2
	Num	10101	11298	15072	16820	11475	12830	6835	7620	21210	23809	13573	15192	7017	7715	12088	13590

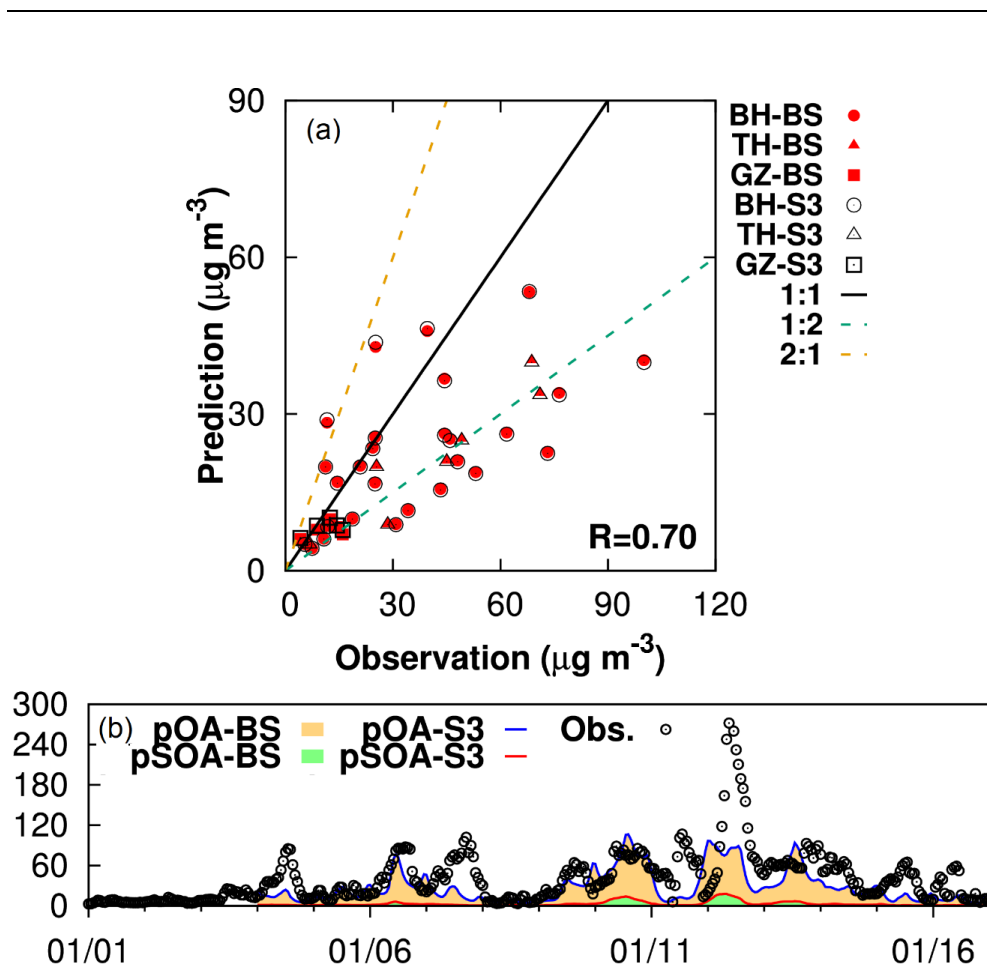


Figure 1. Comparison of (a) observed and modeled organic carbon concentration at University of Beihang (BH), Tsinghua University (TH) and Guangzhou (GZ); (b) observed organic aerosol (Obs.) at Beijing and predictions of total OA (pOA) and SOA (pSOA), unit is $\mu\text{g m}^{-3}$. Locations of monitoring sites are shown in Figure S1.

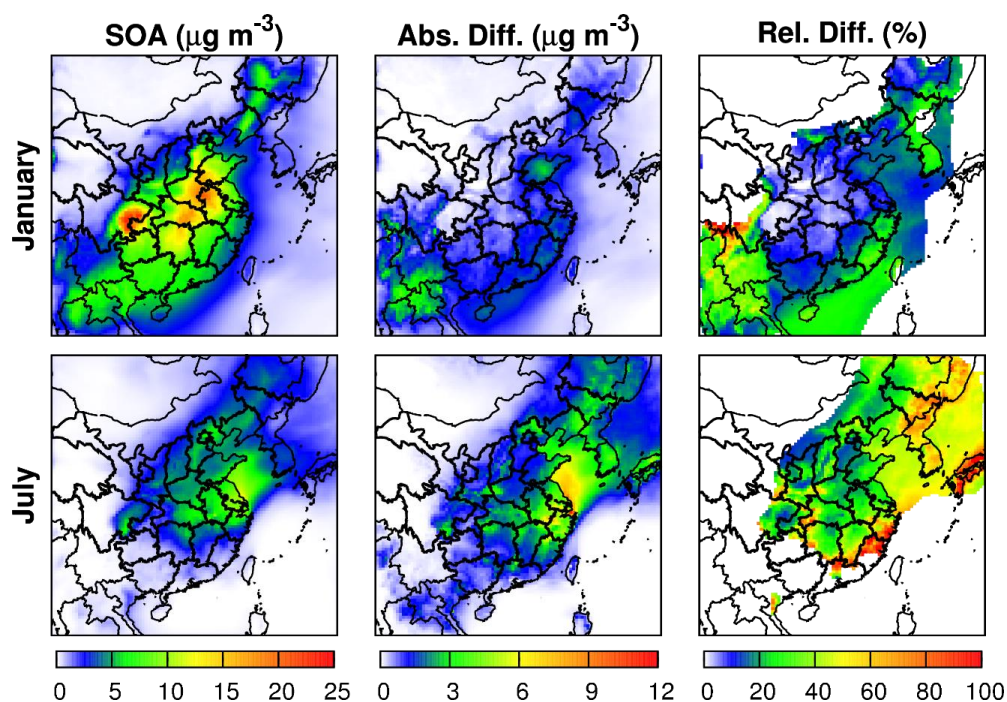


Figure 2. Monthly-averaged total SOA in BS and monthly-averaged daily maximum changes of SOA due to water partitioning and non-ideality of organic-water mixture. “Abs. Diff.” represents absolute differences (S_3 -BS); “Rel. Diff.” represents relative differences ($(S_3$ -BS)/BS, %). Relative differences are shown in areas with monthly-averaged SOA concentration greater than $1 \mu\text{g m}^{-3}$.

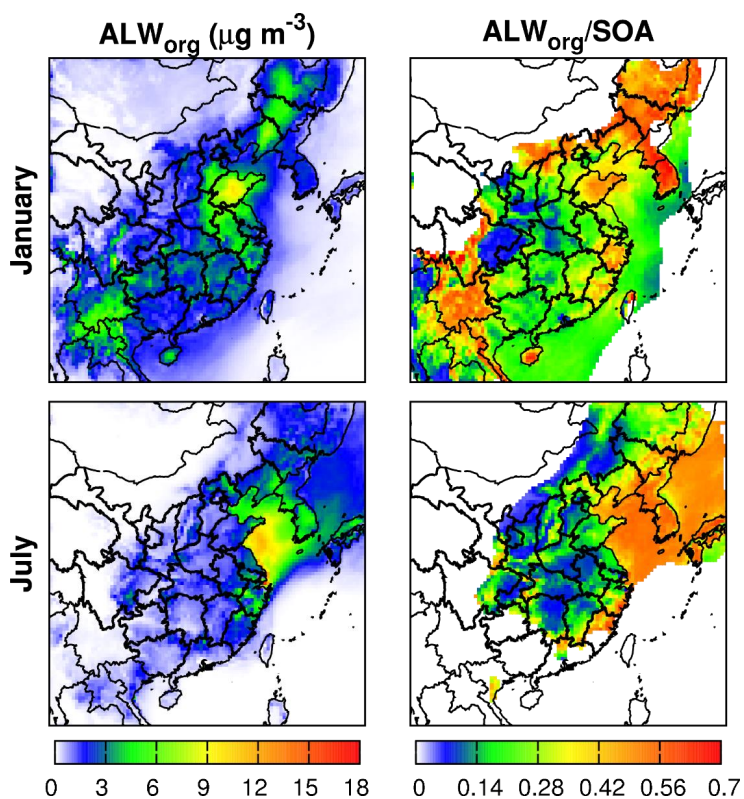


Figure 3. Monthly-averaged daily maximum water partitioning into the organic-phase (ALW_{org} , $\mu\text{g m}^{-3}$) and the ratio to SOA (ALW_{org}/SOA) during January and July of 2013. ALW_{org}/SOA is shown in areas with monthly-averaged SOA concentration greater than $1 \mu\text{g m}^{-3}$.

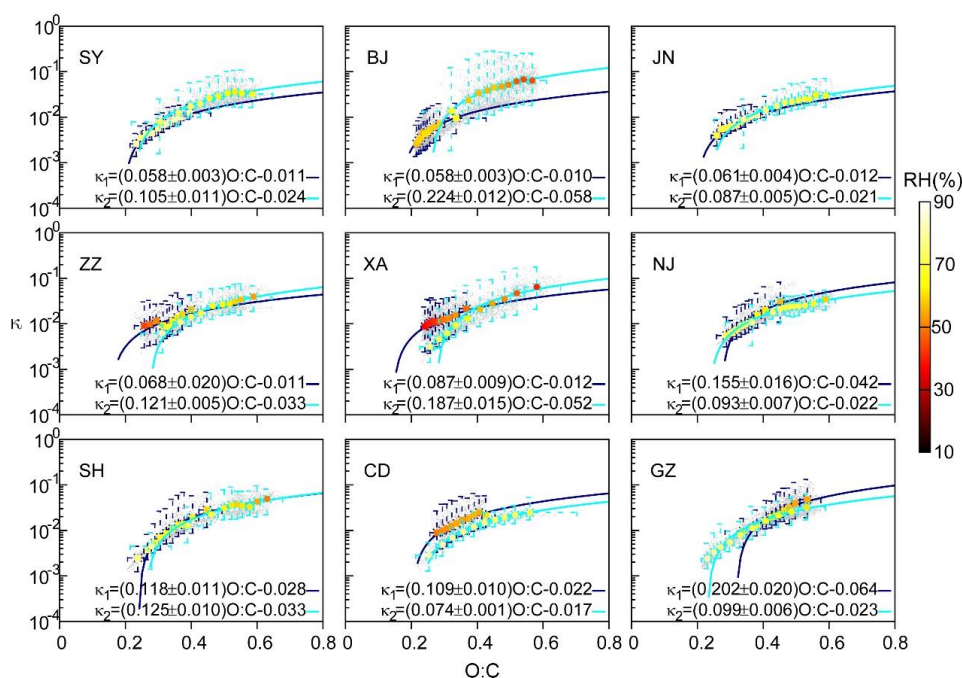


Figure 4 The correlation of hygroscopicity of aerosol (κ) and O:C ratio at 9 representative cities including Shenyang (SS), Beijing (BJ), Jinan (JN), Zhengzhou (ZZ), Xi'an (XA), Nanjing (NJ), Shanghai (SH), Chengdu (CD), and Guangzhou (GZ). Gray dots on the background represent all the data in January and July, which are categorized into several O:C bins. In each bin, the ranges of κ and O:C ratio are represented by dashed bars colored for January (navy) and July (light blue), with the mean value colored by the averaged RH of each bin. The mean κ and O:C ratio are fitted by reduced major axis regression.

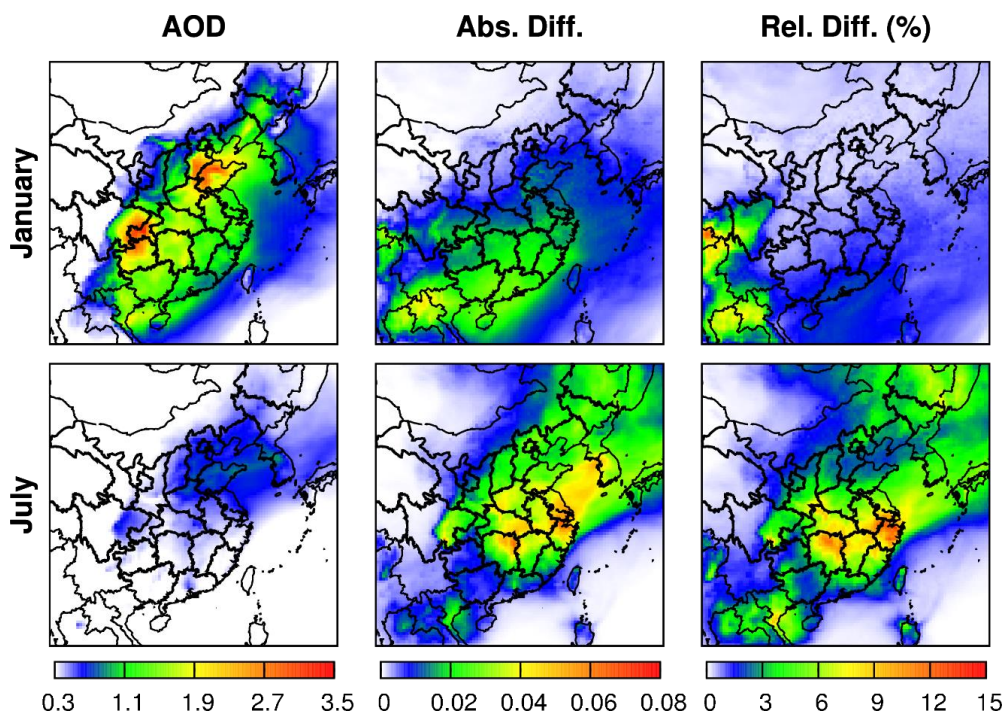


Figure 5. Monthly-averaged AOD_r at 550 nm and the monthly-averaged daily maximum changes of AOD_r due to water partitioning and the non-ideality of organic-water mixture. “Abs. Diff.” represents absolute differences (S3-BS); “Rel. Diff.” represents relative differences ((S3-BS)/BS, %).

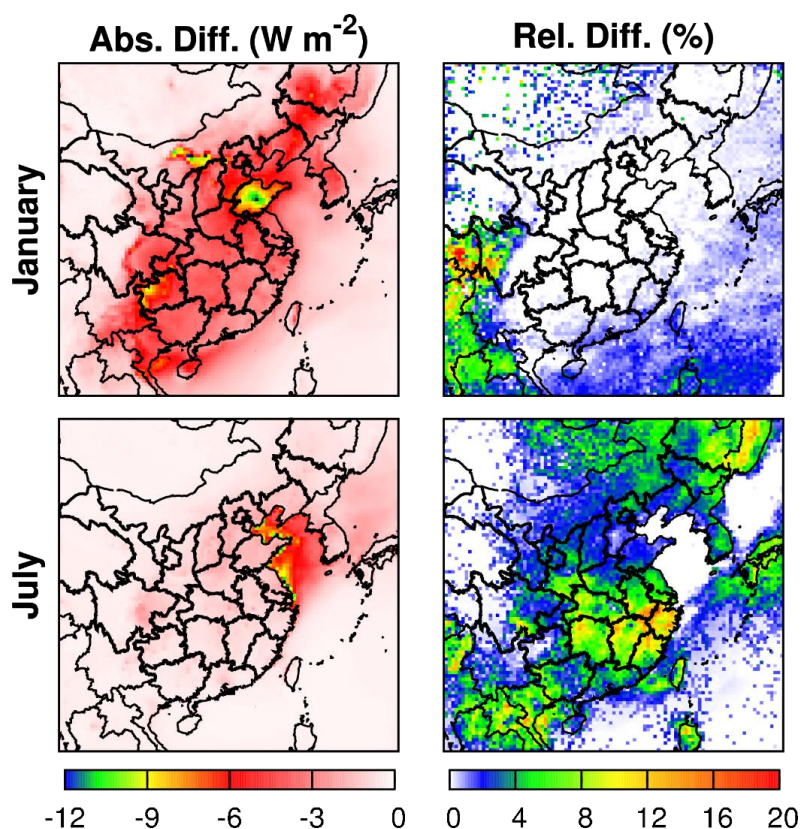


Figure 6. Monthly-averaged daily maximum variation of shortwave direct aerosol radiative forcing at the top of atmosphere due to water partitioning during January and July of 2013. “Abs. Diff.” represents absolute differences (S3-BS); “Rel. Diff.” represents relative differences ((S3-BS)/BS, %).

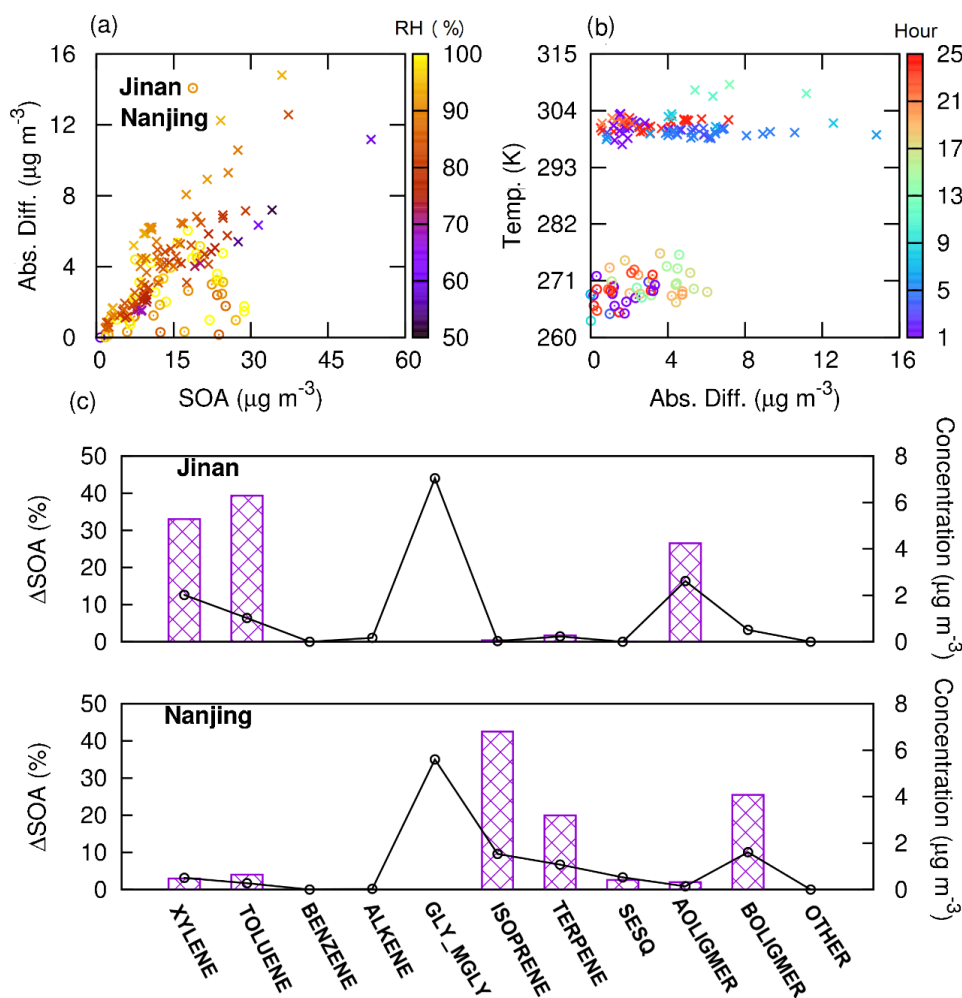


Figure 7. Correlation of water partitioning on SOA with (a) RH (b) temperature at Jinan in winter and Nanjing in summer, and the contribution from each SOA component to the total SOA increase. In plot (a) and (b), “Abs. Diff.” represents the daily maximum change of SOA that is calculated as S3-BS. Color box represents RH in (a) and the hour in the day in (b) when daily maximum change of SOA occurred. In (c), the left axis represents contribution of each SOA component to the daily maximum SOA change due to water partitioning, and the right axis represents the concentration of each SOA component.

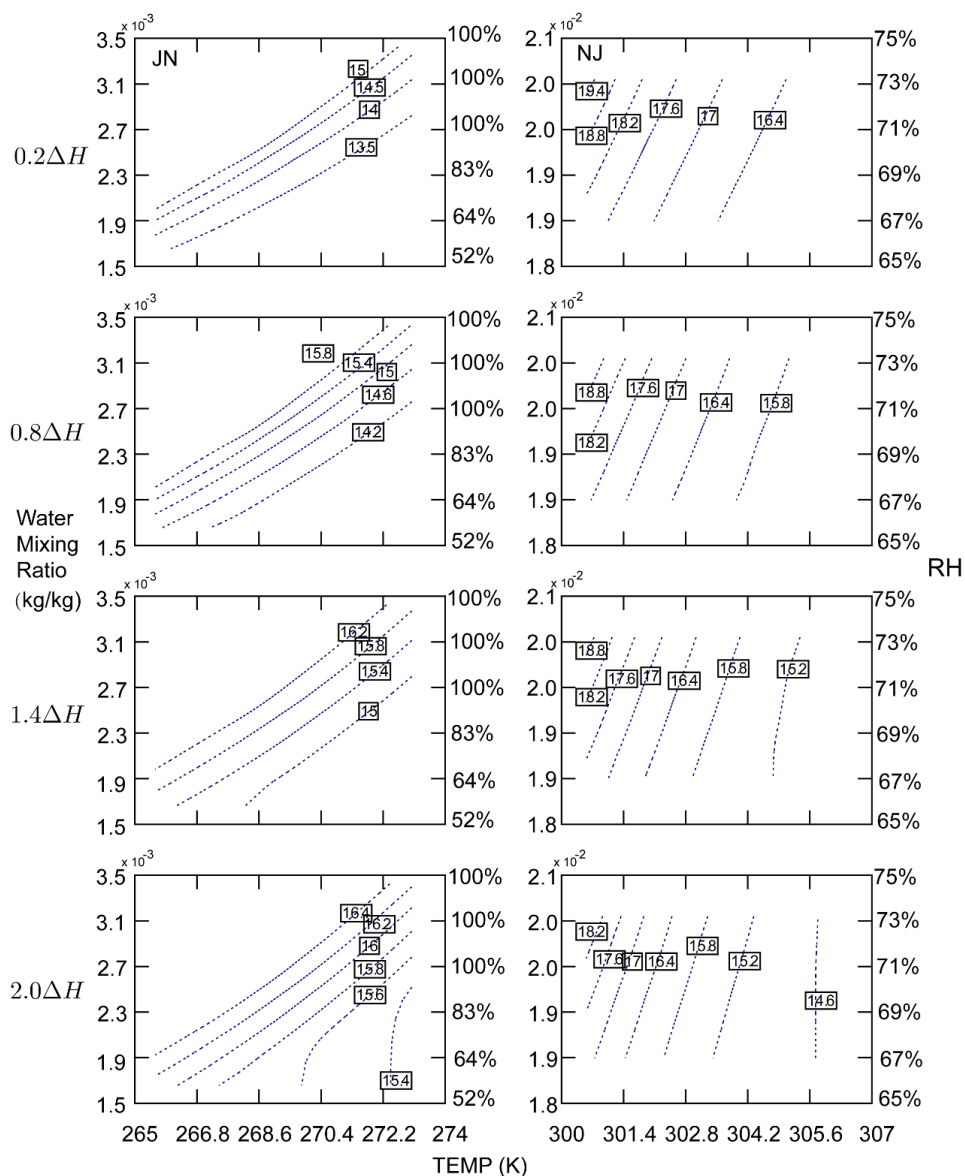


Figure 8. Sensitivity of SOA formation to temperature (TEMP), relative humidity (RH) and the temperature dependence parameter of SVP (ΔH) at Jinan (JN, first column) and Nanjing (NJ, second column). The relative humidity is showing on the right side of y-axis.